

COMPLEX ATTOSECOND TRANSIENT-ABSORPTION SPECTROSCOPY

DISSERTATION

Presented in Partial Fulfillment of the Requirements for the Degree Doctor of
Philosophy in the Graduate School of The Ohio State University

By

Stephen J. Hageman, M.Sc.

Graduate Program in Physics

The Ohio State University

2019

Dissertation Committee:

Louis F. DiMauro, Advisor

Douglass Schumacher

Jay Gupta

Robert Baker

© Copyright by
Stephen J. Hageman
2019

ABSTRACT

The complex dipole is reconstructed in a transient absorption experiment.

Dedicated to coffee

ACKNOWLEDGMENTS

I would like to thank Sir Rickenabcker First of His Name, Last of His Kind, for his eternal indifference.

VITA

June 2011	Bachelors of Science in Physics and Mathematics, Johns Hopkins University
Dec 2014	Master of Science in Physics, The Ohio State University

Publications

“Rapid thermal annealing study of magnetoresistance and perpendicular anisotropy in magnetic tunnel junctions based on MgO and CoFeB”, Wei-Gang Wang, **Stephen Hageman**, *et al.*, Applied Physical Letters. I am a contributing author and performed many of the measurements of magnetoresistance. [Link to electronic version](#).

Table of Contents

	Page
Abstract	ii
Dedication	iii
Acknowledgments	iv
Vita	v
List of Figures	vii
List of Abbreviations	viii

Chapters

1 Two-source high harmonic generation	1
1.1 Introduction	1
1.2 Theory	1
1.2.1 Laser beam shaping using diffractive optics	1
1.2.2 Beam splitting phase grating	5
1.2.3 Square-wave phase grating for high-harmonic generation	11
1.3 Two-source high harmonic generation	16
Appendix A Square-Wave Phase Grating	24
Bibliography	25

List of Figures

Figure	Page
1.1 Schematic demonstrating how to use a diffractive optical element to shape the beam profile at the focal plane. A collimated coherent beam is incident upon a diffractive optical element which shapes the phase of the incident beam, and then a lens is used as a transform element to Fourier transform the beam at the focal plane. The intensity profile at the focal plane can be controlled by altering the spatial dependence of the phase imparted upon the incident beam by the phase element. Adapted from [1]	2
1.2 Plot of the phase function $\phi(x - x_0)$ in units of π for a $0 - \pi$ square-wave phase grating (SWPG) with a period of d . The dark blue curve (light blue) shows the phase function for $x_0 = 0$ ($x_0 = d/10$).	6
1.3 Square complex modulus of the Fourier coefficients a_n of the $0 - \pi$ SWPG. The square complex modulus is proportional to the energy put into each diffraction order. As can be seen from figure, the ± 1 orders have the most energy put into them at $4/\pi^2 \approx 41.1\%$ each. All even orders have zero energy.	8
1.4 Intensity profile $S(\tilde{x})$ at the focal plane. Horizontal units are scaled by the spacing between orders, $\tilde{x}_1 = \lambda f/d$. Phase is also plotted for two different offset positions $x_0 = d/3$ and $x_0 = d/5$. This demonstrates the ability of the SWPG to generate two sources and control the relative phase between them.	9
1.5 Square complex modulus of the Fourier coefficients a_n of the $0 - \pi$ SWPG for several values of ζ . The square complex modulus is proportional to the energy put into each diffraction order. As can be seen from figure, the ± 1 orders have the most energy put into them even for $\zeta \neq 1$. All non-zero even orders have zero energy.	11
1.6 Refractive index (blue curve and axis) and the ζ parameter (red curve and axis). For a 70 nm bandwith pulse centered at 1350 nm, $\zeta - 1$ varies from -0.025 to 0.025 assuming normal incidence.	13
1.7 Non- π phase step parameter $\zeta(\lambda, \theta)$ calculated for a range of relevant wavelengths and incident angles. The ability to effectively tune the optical path length of the step enables the SWPG to be used for a much larger range of wavelengths that are longer than the initial design wavelength.	14

1.8	Calculation of intensity at the focal plane of the SWPG for various parameters of β . Calculation is done my numerically propagating the measured beam profile shown in 1.10. β is varied by adjusting the radius of the input beam profile. As $\beta \rightarrow 0$, one can see that the perfomance of the SWPG deteriorates and not longer produces well separated sources.	15
1.9	Schematic of the two SWPG which were purchased. They are constructed by etching the phase step in Corning HPFS 7980 fused-silica.	17
1.10	Intensity profile of the input beam measured by a thermal camera. Phase imparted by SWPG	17
1.11	reference image and power spectrum of spatial frequencies	18
1.12	reference image and power spectrum of spatial frequencies	19
1.13	full spatialgram	20
1.14	full spatialgram with $\omega - 2\omega$ generation conditions	20
1.15	Camera image of two sources generating a filament in a gas cell. Image was taken while chamber was vented and at ambient pressure.	22
1.16	Camera image of the output of the phosphor screen. Harmonics are visible by eye.	23

Chapter 1

TWO-SOURCE HIGH HARMONIC GENERATION

1.1 Introduction

A common difficulty in working with extreme ultraviolet (XUV) light is the lack of efficient and broadband optics, especially beam splitters. In this chapter, I will introduce a method for generating two sources of XUV light by high harmonic generation using a **SWPG**. This **SWPG** allows for the duplication of an **infrared (IR)** pulse, as well as precise and stable control of the relative phase between the duplicates of the input **IR** pulse. The two most intense duplicates can generate harmonics which will interfere in the far-field. This can be thought of as an inline Mach-Zehnder interferometer with interferometric stability on sub-wavelength level of the high harmonic. The inherent stability of this two-source scheme will be utilized to measure both the real and imaginary parts of the refractive index of a medium.

1.2 Theory

1.2.1 Laser beam shaping using diffractive optics

In many experimental designs, it is advantageous to be able to shape the spatial intensity distribution of light to be something other than a typical Gaussian beam. A common example of this is generating a beam with an approximately constant intensity across its spatial profile (a flat-top beam). For the experiments described herein, we will be interested in duplicating an input beam with relative phase control between the two duplicate beams. Both of these examples are part of the general concept of laser beam shaping. The challenge is to design an optical system such that given an input beam profile $I_{in}(x, y)$ we can generate the desired output beam profile $I_{out}(x, y)$. Ideally, this optical system is designed in such

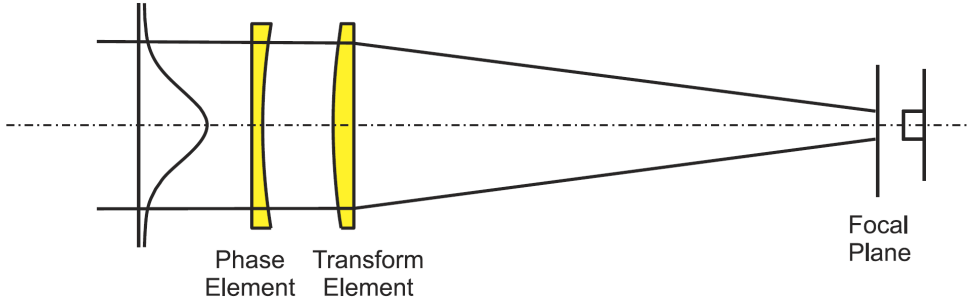


Figure 1.1: Schematic demonstrating how to use a diffractive optical element to shape the beam profile at the focal plane. A collimated coherent beam is incident upon a diffractive optical element which shapes the phase of the incident beam, and then a lens is used as a transform element to Fourier transform the beam at the focal plane. The intensity profile at the focal plane can be controlled by altering the spatial dependence of the phase imparted upon the incident beam by the phase element. Adapted from [1]

a way that it can be nearly lossless.¹ The relevant optical system which will be used is shown in figure 1.1. The system consists of a phase element which modifies the input field by $\phi(x, y)$ and a Fourier transform lens which adds a quadratic phase to the beam to focus it at the focal plane. By appropriate choice of the phase profile of the phase element, one can produce the desired beam profile at the focal plane.

This problem can be theoretically described in terms of Fourier optics [1–3]. If one assumes that a field $u(x, y, 0)$ is incident upon an aperture at $z = 0$, then the field for $z > 0$ can be written under the Fresnel approximation by the Fresnel integral

$$u(x, y, z) = \frac{ik}{2\pi z} e^{ikz} e^{ik(x^2+y^2)/2z} \int_{-\infty}^{\infty} \int_{-\infty}^{\infty} u(\xi, \eta, 0) e^{ik(\xi^2+\eta^2)/2z} e^{-ik(x\xi+y\eta)/z} d\xi d\eta \quad (1.1)$$

where $u(\xi, \eta, 0)$ is the incoming field and $k = 2\pi/\lambda$ is the wavenumber. Now, if one assumes that the phase element is placed at $z = 0$, then immediately after passing through the thin phase element in Fig. 1.1 the field is given by

$$u(\xi, \eta, 0) = f(\xi, \eta) e^{i\phi(\xi, \eta)}. \quad (1.2)$$

After propagating through the thin Fourier transform lens of focal length f , the field at the focal plane is now given by

$$u(x, y, f) = \frac{ik}{2\pi f} e^{ikf} e^{ik(x^2+y^2)/2f} \int_{-\infty}^{\infty} \int_{-\infty}^{\infty} f(\xi, \eta) e^{i\psi(\xi, \eta)} e^{-ik(x\xi+y\eta)/f} d\xi d\eta \quad (1.3)$$

¹In the limit of geometric optics it is possible to make the optical system, in principle, lossless, however this is not generally possible when one considers the wave nature of light.

where

$$\psi(\xi, \eta) = \phi(\xi, \eta) + k(\xi^2 + \eta^2)/2f. \quad (1.4)$$

Now, the idea is to rewrite this field profile at the focal plane into a more intuitive form by introducing the equation

$$g(\xi, \eta) = \frac{ik}{2\pi f} f(\xi, \eta) e^{i\psi(\xi, \eta)}. \quad (1.5)$$

The Fourier transform of this function $g(\xi, \eta)$ is given by

$$G(a, b) = \frac{ik}{2\pi f} \int_{-\infty}^{\infty} \int_{-\infty}^{\infty} f(\xi, \eta) e^{i\psi(\xi, \eta)} e^{-i(a\xi + b\eta)} d\xi d\eta. \quad (1.6)$$

By setting $a = kx/f$ and $b = ky/f$ and taking the square complex modulus, one obtains the equation

$$|G(kx/f, ky/f)|^2 = \frac{k^2}{(2\pi f)^2} \left| \int_{-\infty}^{\infty} \int_{-\infty}^{\infty} f(\xi, \eta) e^{i\psi(\xi, \eta)} e^{-ik(x\xi + y\eta)/f} d\xi d\eta \right|^2. \quad (1.7)$$

By comparing this equation with the square complex modulus of the field at the focal plane (equation 1.3), one finds the relationship

$$|u(x, y, f)|^2 = |G(kx/f, ky/f)|^2. \quad (1.8)$$

From this last equality we have shown that the intensity of the field at the focal plane $|u(z = f)|^2$, is given by the Fourier transform of the combined phase imparted upon the incident field by both the phase element and the Fourier transform lens, $|G|^2$. So, if one wants a specific beam shape $Q(x, y)$ at the focal plane, then by tuning the frequency components of the phase imparted upon the beam $\phi(x, y)$ and the focal length f used then one can achieve the desired beam profile, such that

$$|G(kx/f, ky/f)|^2 = Q(x, y). \quad (1.9)$$

This problem is difficult in general, so the challenge in many beam shaping problems is to try and minimize the error between the true field and the desired field, and to further complicate the matter, many applications will require different notions of error to be used. For example, if one needs the energy distribution to be as close as possible to the desired profile, then the ℓ_2 -norm would be appropriate. However, if the maximum intensity is of concern, then the ℓ_∞ -norm combined with the ℓ_2 -norm would be the appropriate notion of error.

It is possible to gain more insight into how difficult a beam shaping problem will be by reformulating the problem in terms of relevant length scales. The idea is to introduce a dimensionless parameter whose magnitude will reflect the validity of underlying assumptions,

and so for a given value of this parameter one can intuitively understand the performance (or lack thereof) of the beam shaping system. This is done by reformulating the above situation in terms of the natural length scales of both the incoming field and the desired field at the focal plane

$$I_{\text{input}} = |f(x, y)|^2 = |\hat{f}(x/\sigma, y/\sigma)|^2 \quad (1.10)$$

$$I_{\text{desired}} = Q(x, y) = \hat{Q}(x/d, y/d) \quad (1.11)$$

where σ is the characteristic length scale of the input field (typically the beam radius) and d is the characteristic length scale of the desired field. By expressing the fields in this way, we can now introduce the dimensionless parameter

$$\beta = \frac{2\pi\sigma D}{\lambda f}. \quad (1.12)$$

Using this dimensionless parameter, one can rewrite equations 1.6 and 1.9 as

$$G(\chi, \nu) = \int_{-\infty}^{\infty} \int_{-\infty}^{\infty} g(\xi, \eta) e^{-i(\chi\xi + \nu\eta)} e^{i\beta\hat{\psi}(\xi, \eta)} d\xi d\eta \quad (1.13)$$

$$|G(\chi, \nu)|^2 = \frac{4\pi^2 A}{\beta^2} Q(\chi/\beta, \nu/\beta) \quad (1.14)$$

where $\chi = x\sigma k/f$, $\nu = y\sigma k/f$, A is a constant, and $\hat{\psi} = \beta\psi$. From equation 1.2.1, it is clear that the functions g and G are related by a Fourier transform, so they must obey the uncertainty relation given by

$$\mu_g \mu_G \geq 1 \quad (1.15)$$

where μ is the second moment. Now, if one were to choose the phase profile of the phase element $\phi(x, y)$ such that equation 1.14 is satisfied, then one finds that $\mu_G = \beta^2 \mu_Q$. This then leads to the inequality

$$\beta^2 \mu_G \mu_Q \geq 1. \quad (1.16)$$

It can be seen that for large values of β this inequality can be readily satisfied. However, for very small values of β this inequality cannot be met and it will not be possible to produce the desired beam profile. From this, it can be seen that having a large value of β makes the beam shaping problem more tractable. The physical interpretation of β is that it is a measure of validity of geometric optics. It can be shown that when β is large a stationary phase method can be used to expand equation , and the lowest order term can be derived using a geometric optics approximation and higher order terms are related to the effects of diffraction [1, 2].

In this section, the general problem of laser beam shaping has been introduced and formulated as a problem in Fourier analysis, and by rewriting everything in terms of natural length scales we can infer which types of beam shaping problems will be more tractable using

geometrical optics approximations. The discussion so far has been kept very abstract, but in the next section the problem of interest will be introduced and these ideas will become more concrete.

1.2.2 Beam splitting phase grating

Now that the general theory behind laser beam shaping has been introduced, we move on to the specific problem at hand. The idea is to produce two nearly identical XUV beams through [high-harmonic generation \(HHG\)](#) using two nearly identical [IR](#) beams. The challenge is how to produce two nearly identical [IR](#) beams while minimizing the energy lost in the process. An additional requirement is that we can control the relative phase between these two [IR](#) beams. All of these requirements can be met through the use of a beam splitting phase grating.

As shown in section [1.2.1](#), the beam shape at the focal plane of a lens can be controlled through appropriate choice of a phase element and the spatially dependent phase $\phi(x, y)$ which is imparted upon the incoming beam. We will still consider the schematic shown in figure [1.1](#). However, the phase element which will be considered in this section (the beam splitting phase grating) will only modify the phase in one dimension, $\phi(x, y) = \phi(x)$, and it will be a periodic function with a period of d , $\phi(x) = \phi(x + d)$. If we expand the function $P(x) = e^{i\phi(x)}$ in a Fourier expansion

$$P(x) = \sum_{n=-\infty}^{\infty} a_n e^{\frac{i2\pi n x}{d}} \quad (1.17)$$

$$a_n = \frac{1}{d} \int_{-d/2}^{d/2} P(\tilde{x}) e^{-\frac{i2\pi n \tilde{x}}{d}} d\tilde{x}, \quad (1.18)$$

then it can be shown (see Appendix [A](#)) that each of the Fourier coefficients represents a diffracted beam and the energy contained in each diffracted beam is given by the square complex modulus of the Fourier coefficient $|a_n|^2$. Thus, by making our phase element in figure [1.1](#) a phase grating, we have split the beam into many diffraction orders. We have specified the period of the phase grating by requiring $\phi(x) = \phi(x + d)$, however we have not yet determined its shape. This can be accomplished by specifying the distribution of energy into the various diffraction orders. Since we want to split the incoming beam into two duplicate beams, we are searching for d -periodic function such that puts equal energy into two diffraction orders and a maximal amount of the input energy is put into those two orders. It can be shown (see Appendix [A](#)) that the d -periodic function which meets these criteria is a $0 - \pi$ [SWPG](#) given by

$$P(x, x_0) = \text{sign} \left(\cos \left(\frac{2\pi(x - x_0)}{d} \right) \right) \quad (1.19)$$

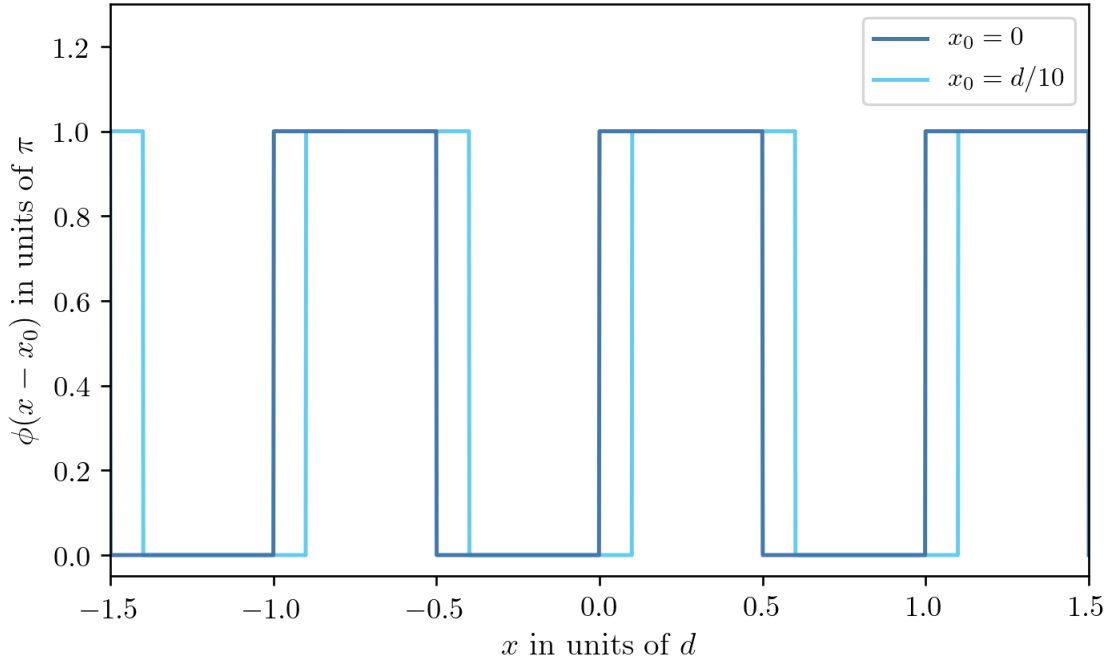


Figure 1.2: Plot of the phase function $\phi(x - x_0)$ in units of π for a $0 - \pi$ SWPG with a period of d . The dark blue curve (light blue) shows the phase function for $x_0 = 0$ ($x_0 = d/10$).

where x_0 is an offset of position of the **SWPG** in the plane transverse to the optical axis. From this equation, it can be seen that the phase of the incoming beam is modulated by either 0 or π , and this is shown in figure 1.2 for $x_0 = 0$ and $x_0 = d/10$.

From equation 1.17, we can calculate the Fourier coefficients $a_n(x_0)$ for the **SWPG** for $n = 0$ and $n \neq 0$. These Fourier coefficients determine how the energy is distributed between the different diffraction orders. For the zeroth-order case ($n = 0$), we find that

$$\begin{aligned} a_0(x_0) &= \frac{1}{d} \int_{-d/2}^{d/2} \text{sign} \left(\cos \left(\frac{2\pi(\tilde{x} - x_0)}{d} \right) \right) d\tilde{x} \\ a_0(x_0) &= \frac{1}{d} \left[- \int_{-\frac{d}{2}}^{-\frac{d}{4} + x_0} d\tilde{x} + \int_{-\frac{d}{4} + x_0}^{\frac{d}{4} + x_0} d\tilde{x} - \int_{\frac{d}{4} + x_0}^{\frac{d}{2}} d\tilde{x} \right] \\ a_0(x_0) &= 0. \end{aligned} \tag{1.20}$$

This demonstrates that zero energy is put into the zeroth-order diffraction for the $0 - \pi$

SWPG. For the other diffraction orders, we find that

$$\begin{aligned}
a_n(x_0) &= \frac{1}{d} \int_{-d/2}^{d/2} \text{sign} \left(\cos \left(\frac{2\pi(\tilde{x} - x_0)}{d} \right) \right) e^{-\frac{i2\pi n \tilde{x}}{d}} d\tilde{x} \\
&= \frac{1}{d} \left[- \int_{-\frac{d}{2}}^{-\frac{d}{4} + x_0} e^{-\frac{i2\pi n x}{d}} d\tilde{x} + \int_{-\frac{d}{4} + x_0}^{\frac{d}{4} + x_0} e^{-\frac{i2\pi n x}{d}} d\tilde{x} - \int_{\frac{d}{4} + x_0}^{\frac{d}{2}} e^{-\frac{i2\pi n x}{d}} d\tilde{x} \right] \\
&= \frac{1}{i2\pi n} \left[e^{\frac{i\pi n}{2} - \frac{i2\pi n x_0}{d}} - e^{in\pi} + e^{\frac{i\pi n}{2} - \frac{i2\pi n x_0}{d}} - e^{-\frac{i\pi n}{2} - \frac{i2\pi n x_0}{d}} + e^{-in\pi} - e^{-\frac{i\pi n}{2} - \frac{i2\pi n x_0}{d}} \right] \\
&= \frac{1}{i\pi n} \left[e^{\frac{i\pi n}{2} - \frac{i2\pi n x_0}{d}} - e^{-\frac{i\pi n}{2} - \frac{i2\pi n x_0}{d}} \right] = \frac{\sin(n\pi/2)}{n\pi/2} e^{-i\frac{2\pi n x_0}{d}} \\
a_n(x_0) &= \text{sinc}\left(\frac{n\pi}{2}\right) e^{-in\frac{2\pi x_0}{d}}.
\end{aligned} \tag{1.21}$$

Since $\text{sinc}(n\pi/2) = 0$ for even integers n , we see that only the odd orders of diffraction from the **SWPG** are populated. The distribution of energy between the different diffraction orders is plotted in figure 1.3, and from this figure it is immediately clear that our choice of the $0 - \pi$ **SWPG** has succeeded in putting most of the input energy equally into two diffraction orders, namely the ± 1 orders. The efficiency of this phase grating can be defined as

$$\eta = |a_1|^2 + |a_{-1}|^2 = \frac{8}{\pi^2} \approx 0.8106, \tag{1.22}$$

which means that approximately 81% of the input energy will be put into the two orders that we want. It should be noted that $\sum_n |a_n|^2 = 1$, which means that while we can't get perfect conversion of energy into only two orders this is still a lossless design.

With these Fourier coefficients in hand, we can now calculate the field profile at the focus. This is done by using equation 1.3

$$\begin{aligned}
\tilde{S}(\tilde{x}) &= \frac{ikA}{2\pi f} e^{ikf} e^{i\frac{k\tilde{x}^2}{2f}} \int_{-\infty}^{\infty} S(x, x_0) e^{-ikx\tilde{x}/f} dx \\
\tilde{S}(\tilde{x}) &= \frac{ikA}{2\pi f} e^{ikf} e^{i\frac{k\tilde{x}^2}{2f}} \int_{-\infty}^{\infty} E(x) \sum_{n=-\infty}^{\infty} a_n(x_0) e^{-i\frac{2\pi n x}{d}} e^{-ikx\tilde{x}/f} dx \\
\tilde{S}(\tilde{x}) &= \frac{ikA}{2\pi f} e^{ikf} e^{i\frac{k\tilde{x}^2}{2f}} \sum_{n=-\infty}^{\infty} a_n(x_0) \int_{-\infty}^{\infty} E(x) e^{-i\frac{2\pi x}{\lambda f} (\tilde{x} - n\frac{\lambda f}{d})} dx \\
\tilde{S}(\tilde{x}) &= \sum_{n=-\infty}^{\infty} a_n(x_0) \tilde{E}(\tilde{x} - \tilde{x}_n)
\end{aligned} \tag{1.23}$$

where

$$\tilde{E}(\tilde{x}) = \frac{ikA}{2\pi f} e^{ikf} e^{i\frac{k\tilde{x}^2}{2f}} \int_{-\infty}^{\infty} E(x) e^{-ikx\tilde{x}/f} dx, \tag{1.24}$$

$x_n = n\lambda f/d$, and A is a constant to account for the y dimension in equation 1.3 which is

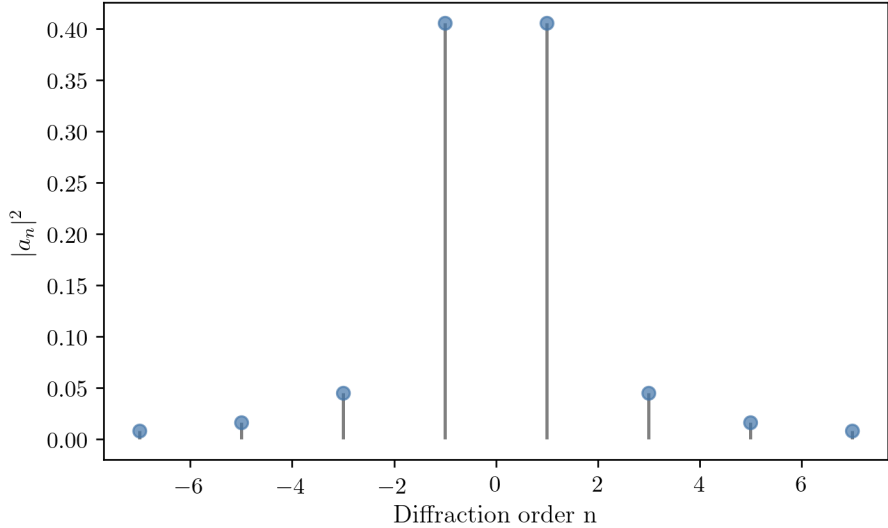


Figure 1.3: Square complex modulus of the Fourier coefficients a_n of the $0 - \pi$ SWPG. The square complex modulus is proportional to the energy put into each diffraction order. As can be seen from figure, the ± 1 orders have the most energy put into them at $4/\pi^2 \approx 41.1\%$ each. All even orders have zero energy.

being neglected for clarity in this discussion. Substituting in equation 1.21 into equation 1.23 yields

$$\tilde{S}(\tilde{x}, x_0) = \sum_{n \neq 0} \text{sinc}\left(\frac{n\pi}{2}\right) \tilde{E}(\tilde{x} - \tilde{x}_n) e^{-in\frac{2\pi x_0}{d}} \quad (1.25)$$

which is the field at the focal plane. From this equation, the role of the transverse offset x_0 immediately becomes clear. It is used to control the relative phase between diffraction orders of the SWPG. The phase difference between the two most populated orders, the $n = \pm 1$, is given by

$$\Delta\phi_{\pm 1} = 2\left(\frac{2\pi x_0}{d}\right). \quad (1.26)$$

Therefore, by controlling the offset of the SWPG we can control the relative phase between the two orders of interest over a range of $[0, 4\pi]$. Additionally, one can begin to see from equation 1.3 that the intensity profile at the focal plane consists of copies of the focused input field at $x_n = n\lambda f/d$. An example intensity profile at the focal plane is shown in figure 1.4. In this figure the ± 1 orders are shown to be the most intense, and the phase is extracted for two different grating offset positions x_0 .

So far, we have demonstrated that a binary $0 - \pi$ SWPG can theoretically achieve our requirements of an efficient beam duplicator with phase control between the two duplicate beams. However, all of the results shown above have been only considering the monochro-

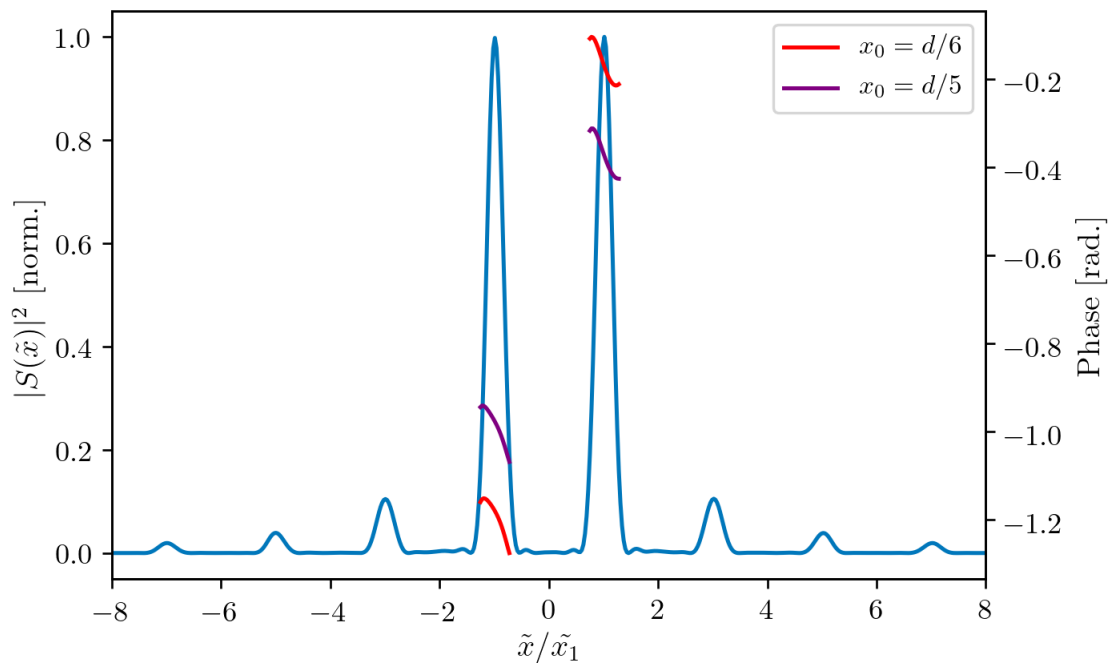


Figure 1.4: Intensity profile $S(\tilde{x})$ at the focal plane. Horizontal units are scaled by the spacing between orders, $\tilde{x}_1 = \lambda f/d$. Phase is also plotted for two different offset positions $x_0 = d/3$ and $x_0 = d/5$. This demonstrates the ability of the **SWPG** to generate two sources and control the relative phase between them.

matic case, and for the experiments of interest we will use a femtosecond **IR** pulse with bandwidth on the order of 50 nm. This presents a challenge because the **SWPG** will be constructed by etching a fused-silica plate to have the desired phase step of π , and the inherent dispersion as the beam passes through the material means that the step will be π for only one wavelength. Thus, it is important to get a handle on how an imperfect phase step affects the properties of the **SWPG**. To do this, we introduce a non- π phase step into the above analysis by a parameter ζ , such that

$$\phi(x, x_0, \zeta) = \zeta \phi(x, x_0). \quad (1.27)$$

Going back to 1.20, we can calculate the zero-order term for $\zeta \neq 1$.

$$\begin{aligned} a_0(x_0, \zeta) &= \frac{1}{d} \int_{-\frac{d}{2}}^{\frac{d}{2}} e^{\zeta \phi(\tilde{x}, x_0)} d\tilde{x} \\ &= \frac{1}{d} \left[\int_{-\frac{d}{2}}^{-\frac{d}{4}+x_0} e^{i\zeta\pi} d\tilde{x} + \int_{-\frac{d}{4}+x_0}^{\frac{d}{4}+x_0} d\tilde{x} + \int_{\frac{d}{4}+x_0}^{\frac{d}{2}} e^{i\zeta\pi} d\tilde{x} \right] \\ &= \frac{1}{d} \left[\frac{d}{2} + \frac{d}{2} e^{i\zeta\pi} \right] = \frac{e^{i\zeta\pi/2}}{2} \left[e^{i\zeta\pi/2} + e^{-i\zeta\pi/2} \right] \\ a_0 &= \cos\left(\frac{\pi}{2}\zeta\right) e^{i\zeta\pi/2} \end{aligned} \quad (1.28)$$

Previously, for $\zeta = 1$ we found that the zeroth order term was not populated by the **SWPG** ($a_0 = 0$), however from the above equation we can clearly see that the non- π phase step has introduced a population in the zeroth order. The percent of the total input energy that is placed into the zeroth order is $|a_0(\zeta)| = \cos^2(\zeta\pi/2)$. Furthermore, from equation 1.21 we can also calculate the other orders for $\zeta \neq 1$.

$$\begin{aligned} a_n(x_0, \zeta) &= \frac{1}{d} \int_{-\frac{d}{2}}^{\frac{d}{2}} e^{\zeta \phi(\tilde{x}, x_0)} e^{-in\frac{2\pi\tilde{x}}{d}} d\tilde{x} \\ &= \frac{1}{d} \left[\int_{-\frac{d}{2}}^{-\frac{d}{4}+x_0} e^{i\zeta\pi - in\frac{2\pi\tilde{x}}{d}} d\tilde{x} + \int_{-\frac{d}{4}+x_0}^{\frac{d}{4}+x_0} e^{-in\frac{2\pi\tilde{x}}{d}} d\tilde{x} + \int_{\frac{d}{4}+x_0}^{\frac{d}{2}} e^{i\zeta\pi - in\frac{2\pi\tilde{x}}{d}} d\tilde{x} \right] \\ a_n(x_0, \zeta) &= \text{sinc}\left(\frac{n\pi}{2}\right) \sin\left(\frac{\pi}{2}\zeta\right) e^{i\frac{\pi}{2}(\zeta-1)} e^{-in\frac{2\pi x_0}{d}} \\ a_n(x_0, \zeta) &= a_n(x_0) \sin\left(\frac{\pi}{2}\zeta\right) e^{i\frac{\pi}{2}(\zeta-1)} \end{aligned} \quad (1.29)$$

From this equation, we can see that the non- π phase step has not populated the even diffraction orders, but the odd orders have an overall phase shift and are reduced in amplitude by a factor of $\sin(\zeta\pi/2)$. This should be expected because we saw from equation 1.28 that the zeroth order was populated by a fractional energy of $|\cos(\zeta\pi/2)|^2$. Since this is a lossless system ($\sum_n |a_n|^2 = 1$), the energy that is populating the zeroth order is coming from all of

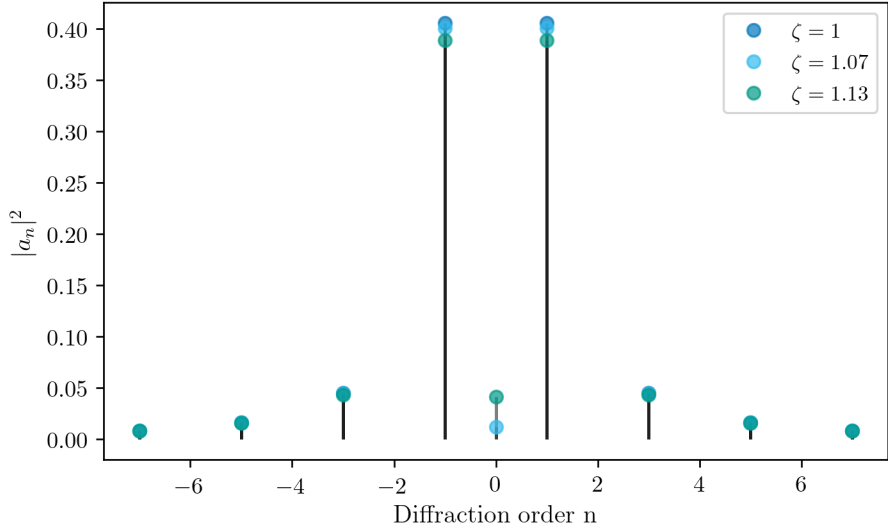


Figure 1.5: Square complex modulus of the Fourier coefficients a_n of the $0 - \pi$ SWPG for several values of ζ . The square complex modulus is proportional to the energy put into each diffraction order. As can be seen from figure, the ± 1 orders have the most energy put into them even for $\zeta \neq 1$. All non-zero even orders have zero energy.

the odd orders that were populated. This redistribution of energy by $\zeta \neq 1$ is shown in 1.5.

From equations 1.28 and 1.29, we now have a notion of how the SWPG is behaving across the bandwidth of our femtosecond pulses. In particular, so long as ζ is close to 1, then the ± 1 orders are still the most intense, and as the grating offset x_0 is varied the phase difference between the ± 1 orders remains $\Delta\phi_{\pm 1} = 2\left(\frac{2\pi x_0}{d}\right)$ even though the overall spectral phase is modified by a factor of $e^{i\zeta\pi/2}$. To set a scale for what ζ close to 1 means, consider the case when the zeroth order is equal in amplitude to the the ± 3 orders, $|a_0(x_0, \zeta)| = |a_{\pm 3}(x_0, \zeta)|$. In this case, $|\xi - 1| = |\frac{2}{\pi} \tan^{-1}(3\pi/2) - 1| \approx 0.13$. Therefore, it is reasonable to state the $0 - \pi$ SWPG maintains its phase control duplication properties for $|\zeta - 1| < 0.13$.

1.2.3 Square-wave phase grating for high-harmonic generation

With the theory behind the SWPG well established, the specific grating parameters that were chosen with HHG in mind will be discussed in this section. The laser source that will be considered is the output of a HE-TOPAS optical parametric amplifier produced by Light Conversion. The TOPAS is pumped by a Spitfire ACE Ti:Sapphire system from Spectra-Physics. The Spitfire ACE system is capable of producing 12 mJ, 60 fs (20 nm FWHM bandwidth) pulses at 1 kHz. Using this system, the TOPAS is able to generate up to a combined 6 mJ of signal and idler. The signal range is from 1200 nm to 1600 nm,

and within this range the TOPAS can output a nominally 70 fs pulse of up to 3 mJ with a tuneable central wavelength. A design wavelength of 1350 nm was chosen for the **SWPG** because the TOPAS performance is optimal around this wavelength.

Once the design wavelength for the phase grating is selected, then the physical size, L , of the step is determined by dispersion of the material selected by the relationship $\phi = \pi = 2\pi nL/\lambda$. For our phase gratings, Corning HPFS 7980 was used, and with this material $L \approx 0.466\mu m$. The refractive index and the corresponding ζ parameter is shown in figure 1.6. The limitation that $\zeta = 1$ for only the design wavelength can be relaxed somewhat by introducing a nonzero angle of incidence between the incoming beam and the **SWPG** to effectively increase the optical path length of the step. If this angle is θ , then the ζ parameter can be written as

$$\zeta(\lambda, \theta) = \sec \theta \left(\frac{n(\lambda)\lambda_0}{\lambda n_0} \right) \quad (1.30)$$

where λ_0 is the design wavelength and n_0 is the refractive index at the design wavelength. This factor is shown in figure 1.6. From this figure, it is clear that even though the **SWPG** is designed for a specific wavelength it can be used over a broad range of wavelengths that are longer than the design wavelength. Of course, at higher angles of incidence propagation effects might be non-negligible, and those effects are neglected here.

The final remaining design parameter that must be considered is the choice of grating period. The choice of period is critical for the performance of the **SWPG**, and must be chosen with care. To get insight into how to select the correct period, we will reintroduce the β parameter from equation 1.12. For the specific situation we are considering, the β parameter is

$$\begin{aligned} \beta &= \frac{2\pi\sigma D}{\lambda f} = \frac{2\pi\sigma(\frac{\lambda f}{d})}{\lambda f} \\ &= 2\pi\left(\frac{\sigma}{d}\right) \end{aligned} \quad (1.31)$$

where σ is the input beam radius and $D = \tilde{x}_1 = \lambda f/d$ is that characteristic length scale at the focal plane because it represents the separation between the different diffraction orders in the focal plane. The beam profile at the focus can be calculated for various parameters of β , and is shown in figure 1.8. In the limit as $\beta \rightarrow 0$ the condition $d \gg \sigma$ must hold, and this condition implies that the source separation is approaching the waist radius of each diffraction order $\tilde{\sigma}$. Once the separation between orders becomes comparable to the separation between orders ($\tilde{\sigma} \approx \tilde{x}_1$), then each diffraction order will strongly interfere with its neighboring orders. The effect of the interference is that our sources can no longer be thought of as independent beams, and as the grating offset x_0 is varied there will be a strong modulation of both the amplitude and phase of each of diffraction order. This can be seen

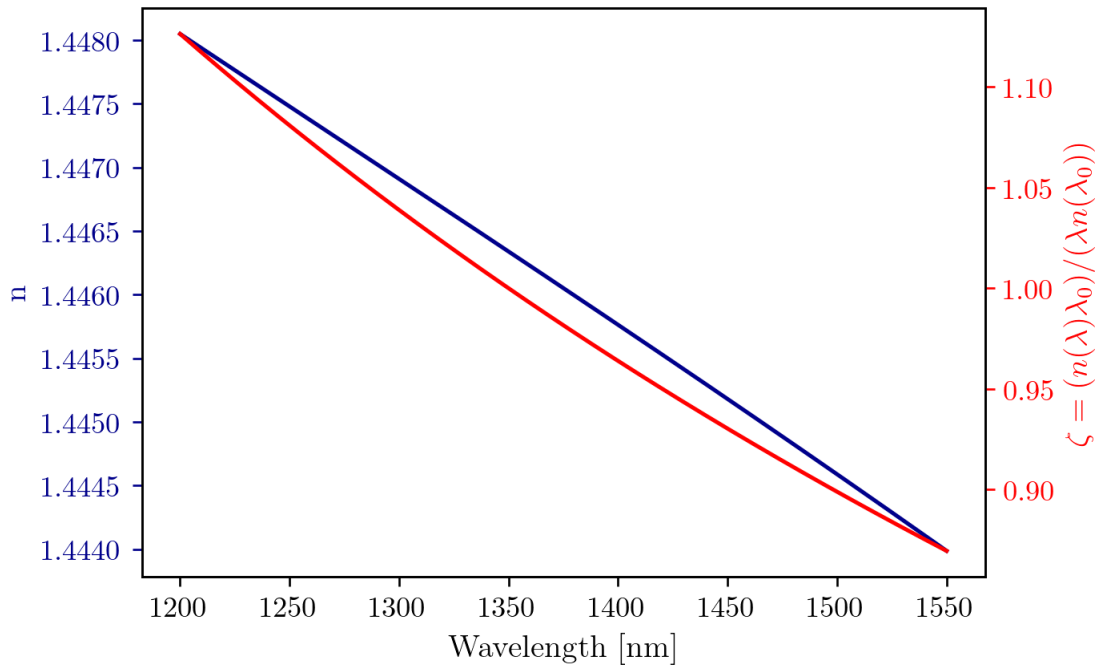


Figure 1.6: Refractive index (blue curve and axis) and the ζ parameter (red curve and axis). For a 70 nm bandwith pulse centered at 1350 nm, $\zeta - 1$ varies from -0.025 to 0.025 assuming normal incidence.

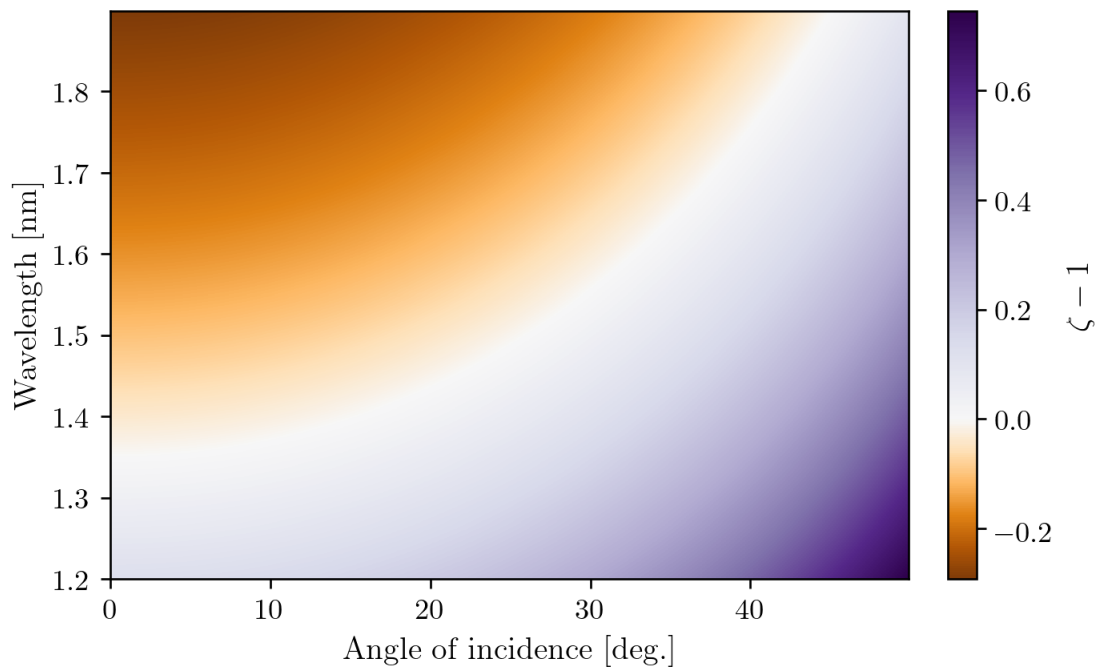


Figure 1.7: Non- π phase step parameter $\zeta(\lambda, \theta)$ calculated for a range of relevant wavelengths and incident angles. The ability to effectively tune the optical path length of the step enables the [SWPG](#) to be used for a much larger range of wavelengths than are longer than the initial design wavelength.

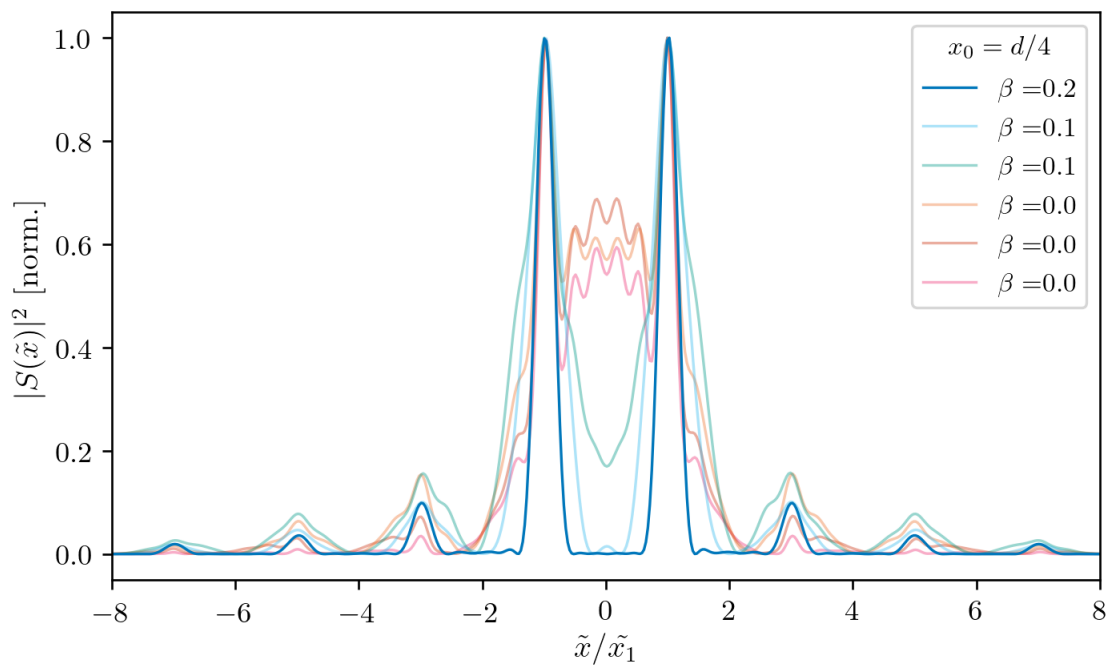


Figure 1.8: Calculation of intensity at the focal plane of the **SWPG** for various parameters of β . Calculation is done by numerically propagating the measured beam profile shown in 1.10. β is varied by adjusting the radius of the input beam profile. As $\beta \rightarrow 0$, one can see that the performance of the **SWPG** deteriorates and no longer produces well separated sources.

by using equation 1.23 to write the intensity at the focal plane

$$\begin{aligned}
|\tilde{S}(\tilde{x}, \phi_1)|^2 &= \sum_{n=-\infty}^{\infty} \sum_{n'=-\infty}^{\infty} a_n \tilde{E}(\tilde{x} - \tilde{x}_n) e^{-in\phi_1} a_{n'} \tilde{E}(\tilde{x} - \tilde{x}_{n'}) e^{-in'\phi_1} \\
&= \sum_{q=-\infty}^{\infty} e^{-iq\phi_1} \sum_{n=-\infty}^{\infty} a_n \tilde{E}(\tilde{x} - \tilde{x}_n) a_{n-q} \tilde{E}(\tilde{x} - \tilde{x}_{n-q}) \\
&= \sum_{n=-\infty}^{\infty} \tilde{E}_{2n+1}^2(\tilde{x}) + 2 \sum_{q=1}^{\infty} \cos(2q\phi_1) \sum_{n=-\infty}^{\infty} \tilde{E}_{2n+1}(\tilde{x}) \tilde{E}_{2n-2q+1}(\tilde{x})
\end{aligned} \tag{1.32}$$

where $\tilde{E}_n(\tilde{x}) = |a_n| \tilde{E}(\tilde{x} - \tilde{x}_n)$. The second term demonstrates that as the grating offset x_0 is varied, the intensity of a diffraction order $2n + 1$ will be modulated by an oscillatory term $\cos(2q\phi_1)$. The amplitude of this oscillation is determined by the overlap of the diffraction orders. Thus, for a grating such that $d \gg \sigma$ the oscillations will be very large because the source separation will be comparable to the beam waist of each order.

While it has become clear that choosing a grating period such that $\sigma \gg d$ is the ideal case for the performance of the SWPG as a beam duplicator, there is another consideration that must be made for our particular application. In particular, we would like to generate high-harmonics from the ± 1 orders, and in order to do that we must send both sources through a gas medium generated by a supersonic gas jet. This becomes increasingly difficult to handle as the source separation becomes large because the nozzle diameter must also increase. Since this needs to be done in vacuum, at a certain point the pumping requirements become untenable. So, in light of these considerations, the grating periods that were chosen were 2.5 mm and 3.5 mm. A schematic of the gratings are shown in figure 1.9. Using these gratings and a $f = 400$ mm lens at 1450 nm, we are able to achieve a source separation of $331 \mu\text{m}$ and $464 \mu\text{m}$ for the $d = 3.5$ mm and $d = 2.5$ mm. These parameters correspond to $\beta \approx 7$ for the 3.5 mm grating and $\beta \approx 10$ for the 2.5 mm grating for an input beam radius of $\sigma = 4$ mm.

1.3 Two-source high harmonic generation

$$\begin{aligned}
I_{IR} &= a + b \times \cos(\phi(x_0)) \\
I_q &= \alpha_q \times a^q \left(1 + N_q \frac{b}{a} \cos(\phi(x_0)) \right) + o(b \times a^{q-1})
\end{aligned} \tag{1.33}$$

$$\begin{aligned}
I_{IR}(\tilde{x}_1, x_0) &= |\tilde{S}(\tilde{x}_1, x_0)|^2 \\
&= \left| a_{-1} \tilde{E}(2\tilde{x}_1) + a_0 \tilde{E}(\tilde{x}_1) + a_1 \tilde{E}(0) + a_3 \tilde{E}(2\tilde{x}_1) \right|^2 \\
&= \left| a_0 \tilde{E}(\tilde{x}_1) + a_1 \tilde{E}(0) \right|^2
\end{aligned} \tag{1.34}$$

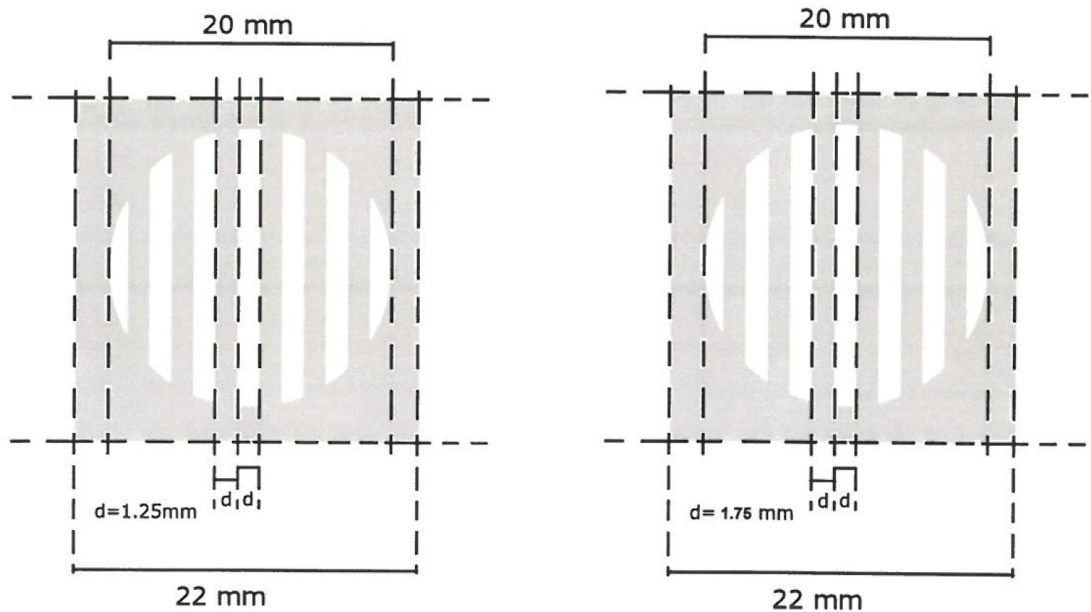


Figure 1.9: Schematic of the two [SWPG](#) which were purchased. They are constructed by etching the phase step in Corning HPFS 7980 fused-silica.

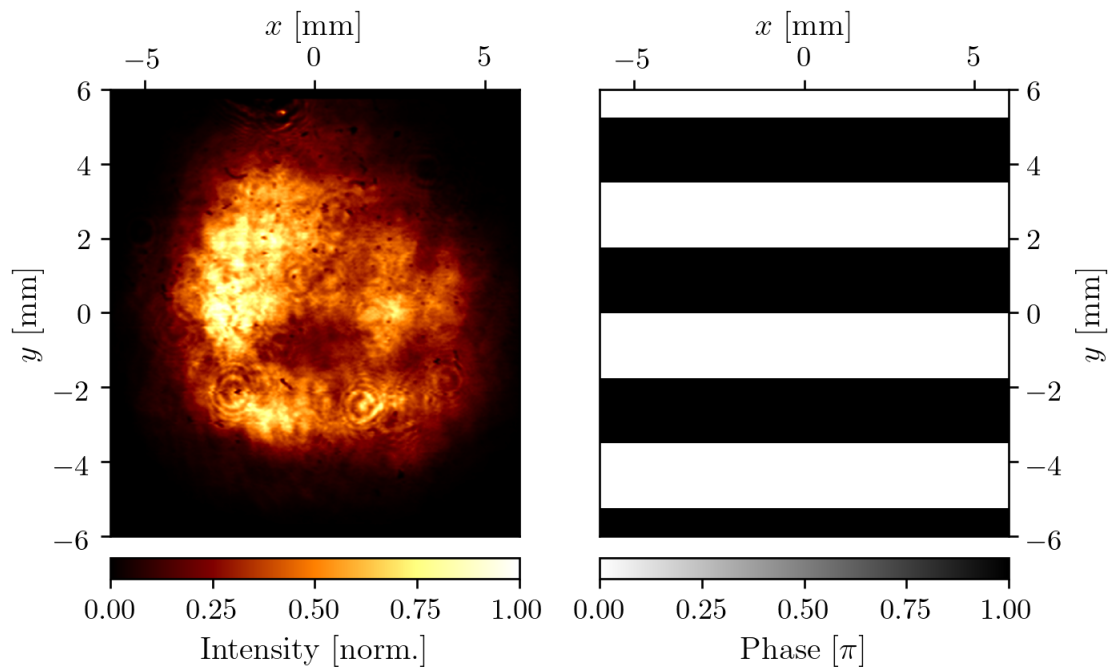


Figure 1.10: Intensity profile of the input beam measured by a thermal camera. Phase imparted by [SWPG](#)

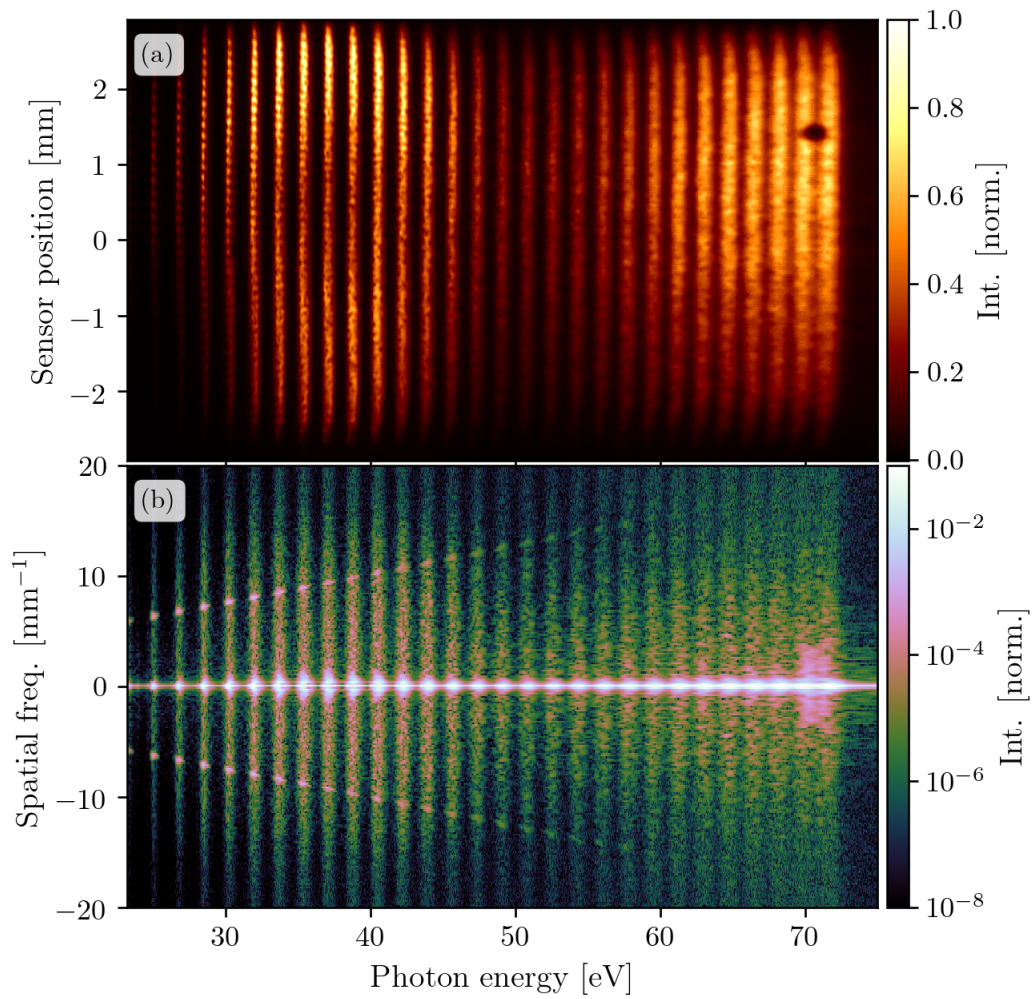


Figure 1.11: reference image and power spectrum of spatial frequencies

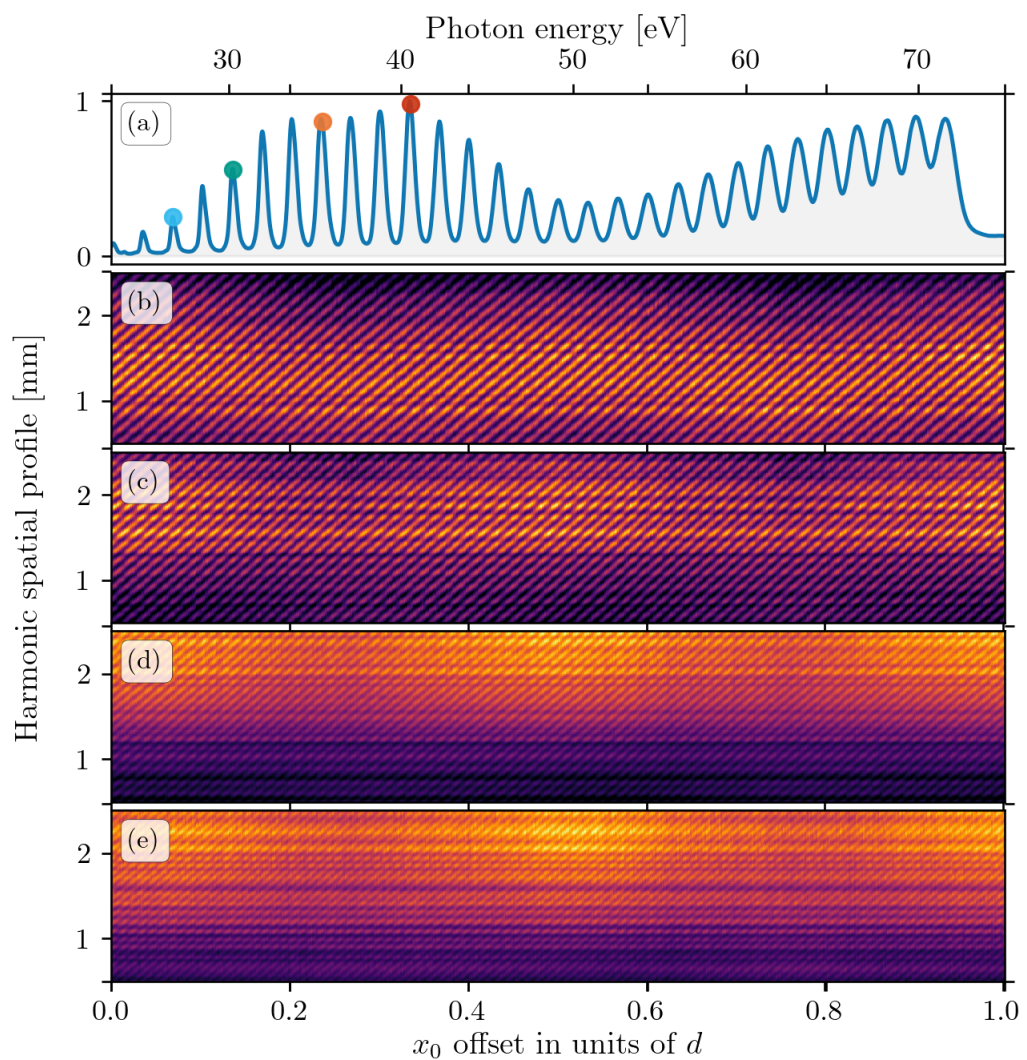


Figure 1.12: reference image and power spectrum of spatial frequencies

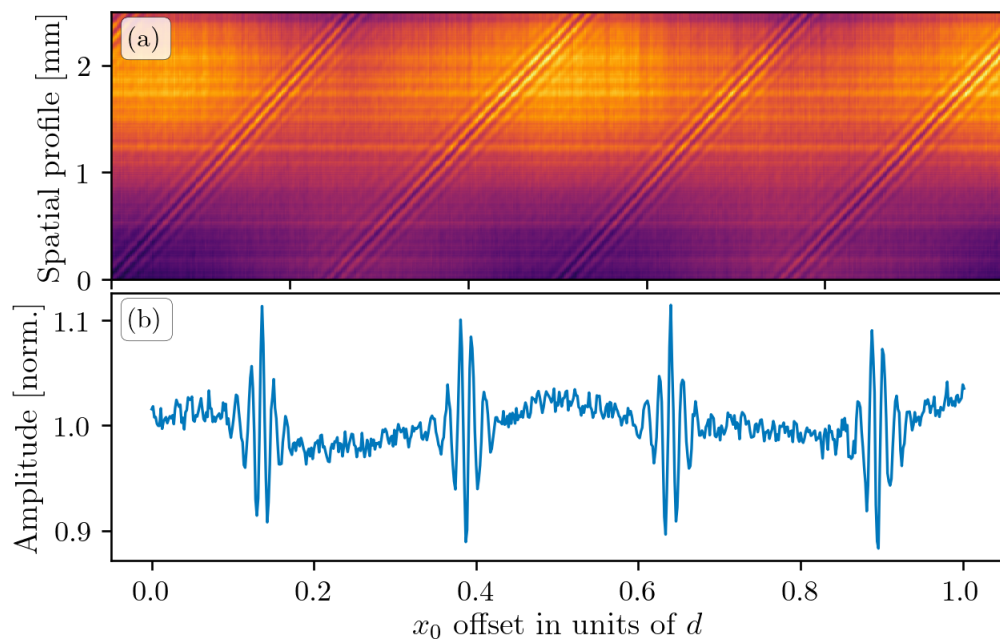


Figure 1.13: full spatialgram

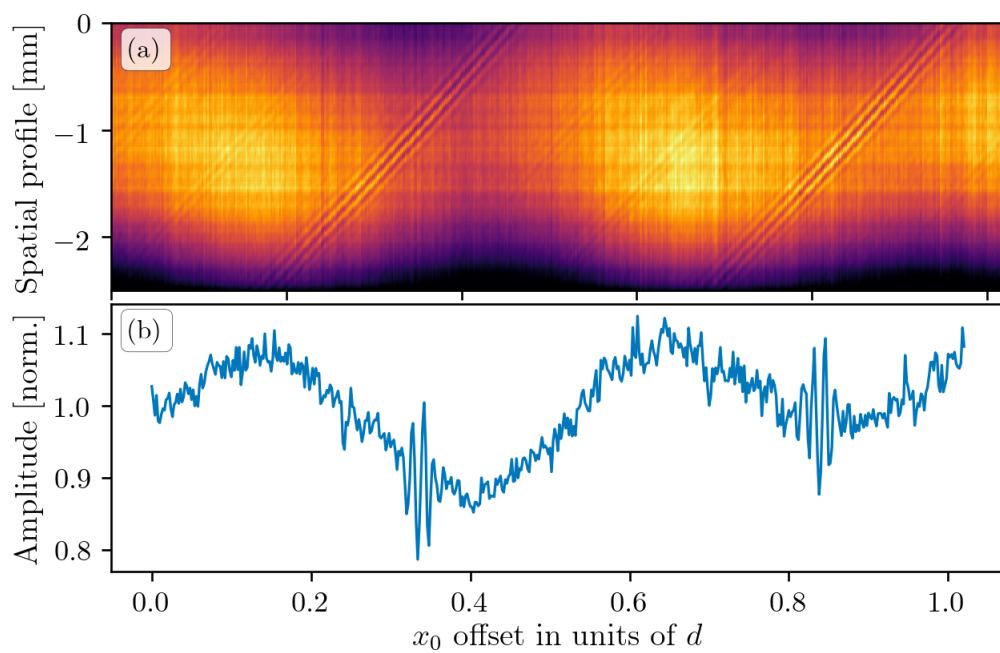


Figure 1.14: full spatialgram with $\omega - 2\omega$ generation conditions

$$I_{IR}(\tilde{x}_1, x_0) = \left| \tilde{E}(0) \right|^2 \left| \frac{2}{\pi} \sin\left(\xi \frac{\pi}{2}\right) e^{i(\xi \frac{\pi}{2} - \phi_1)} + \cos\left(\xi \frac{\pi}{2}\right) e^{i\xi \frac{\pi}{2}} \frac{\tilde{E}(\tilde{x}_1)}{\tilde{E}(0)} - \frac{2 \sin\left(\xi \frac{\pi}{2}\right)}{\pi} e^{i(\xi \frac{\pi}{2} + \phi_1)} \frac{\tilde{E}(2\tilde{x}_1)}{\tilde{E}(0)} + \frac{2 \sin\left(\xi \frac{\pi}{2}\right)}{3\pi} \right| \quad (1.35)$$

$$\begin{aligned} I_{IR}(\tilde{x}_1, x_0) &= \left| \tilde{E}(0) \frac{2}{\pi} \sin\left(\xi \frac{\pi}{2}\right) \right|^2 \left| e^{-i\phi_1} + \frac{\pi}{2 \tan\left(\xi \frac{\pi}{2}\right)} \frac{\tilde{E}(\tilde{x}_1)}{\tilde{E}(0)} - e^{i\phi_1} \frac{\tilde{E}(2\tilde{x}_1)}{\tilde{E}(0)} + \frac{e^{-3i\phi_1}}{3} \frac{\tilde{E}(2\tilde{x}_1)}{\tilde{E}(0)} \right|^2 \\ &= \left| \tilde{E}(0) \frac{2}{\pi} \sin\left(\xi \frac{\pi}{2}\right) \right|^2 \left(1 + \frac{\pi}{\tan\left(\xi \frac{\pi}{2}\right)} \frac{\tilde{E}(\tilde{x}_1)}{\tilde{E}(0)} \cos(\phi_1) - \frac{4}{3} \frac{\tilde{E}(2\tilde{x}_1)}{\tilde{E}(0)} \cos(2\phi_1) \right) \\ I_{IR}(\tilde{x}_{-1}, x_0) &= \left| \tilde{S}(\tilde{x}_{-1}, x_0) \right|^2 \\ &= \left| a_{-1} \tilde{E}(0) + a_0 \tilde{E}(\tilde{x}_1) \right|^2 \\ &= \left| \tilde{E}(0) \right|^2 \left| -\frac{2}{\pi} \sin\left(\xi \frac{\pi}{2}\right) e^{i(\xi \frac{\pi}{2} + \phi_1)} + \cos\left(\xi \frac{\pi}{2}\right) e^{i\xi \frac{\pi}{2}} \frac{\tilde{E}(\tilde{x}_1)}{\tilde{E}(0)} + \frac{2 \sin\left(\xi \frac{\pi}{2}\right)}{\pi} e^{i(\xi \frac{\pi}{2} - \phi_1)} \frac{\tilde{E}(2\tilde{x}_1)}{\tilde{E}(0)} - \frac{2 \sin\left(\xi \frac{\pi}{2}\right)}{3\pi} \right| \\ &= \left| \tilde{E}(0) \frac{2}{\pi} \sin\left(\xi \frac{\pi}{2}\right) \right|^2 \left| e^{-i\phi_1} - \frac{\pi}{2 \tan\left(\xi \frac{\pi}{2}\right)} \frac{\tilde{E}(\tilde{x}_1)}{\tilde{E}(0)} - e^{i\phi_1} \frac{\tilde{E}(2\tilde{x}_1)}{\tilde{E}(0)} + \frac{e^{-3i\phi_1}}{3} \frac{\tilde{E}(2\tilde{x}_1)}{\tilde{E}(0)} \right|^2 \\ &= \left| \tilde{E}(0) \frac{2}{\pi} \sin\left(\xi \frac{\pi}{2}\right) \right|^2 \left(1 - \frac{\pi}{\tan\left(\xi \frac{\pi}{2}\right)} \frac{\tilde{E}(\tilde{x}_1)}{\tilde{E}(0)} \cos(\phi_1) - \frac{4}{3} \frac{\tilde{E}(2\tilde{x}_1)}{\tilde{E}(0)} \cos(2\phi_1) \right) \\ a_0^\xi(x_0) &= \cos\left(\xi \frac{\pi}{2}\right) e^{i\xi \frac{\pi}{2}} \end{aligned} \quad (1.36)$$

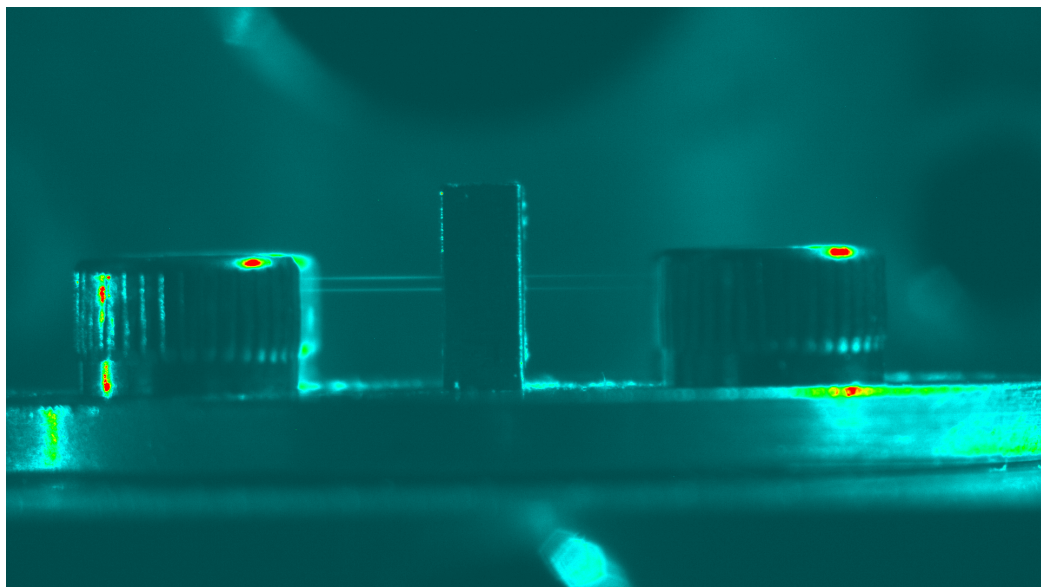


Figure 1.15: Camera image of two sources generating a filament in a gas cell. Image was taken while chamber was vented and at ambient pressure.

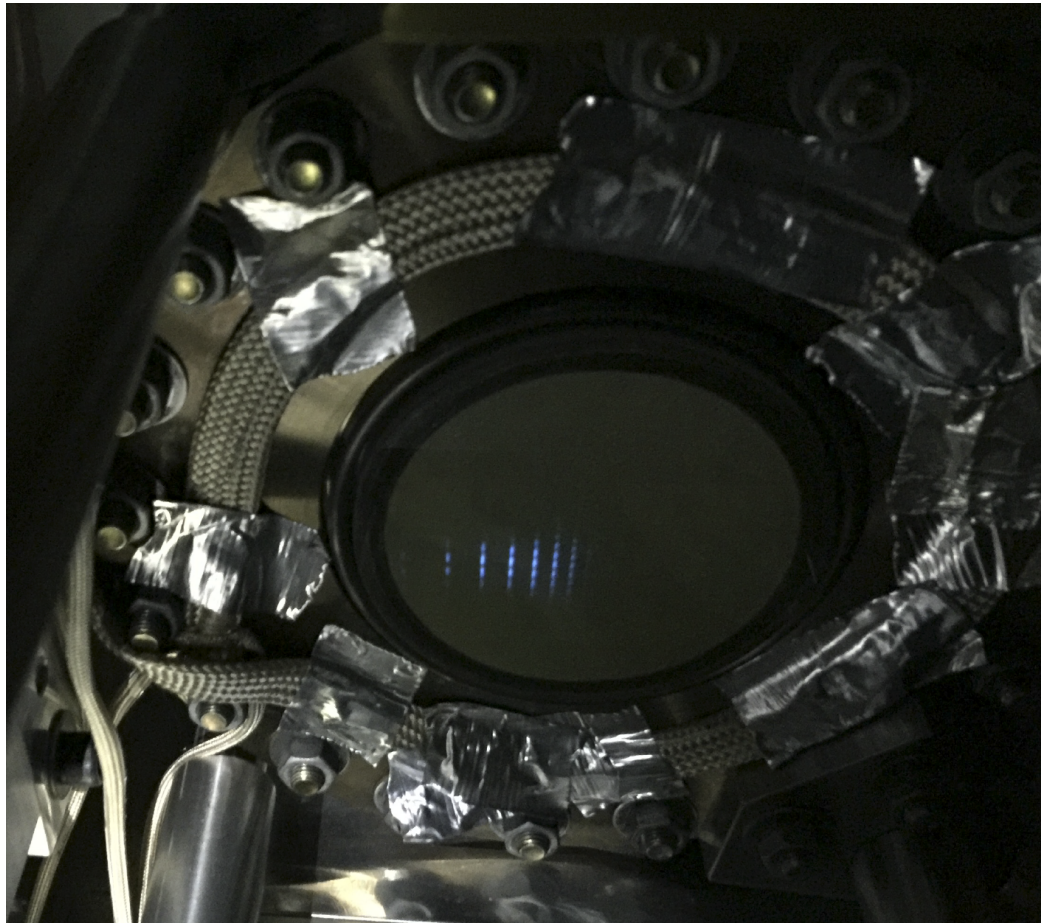


Figure 1.16: Camera image of the output of the phosphor screen. Harmonics are visible by eye.

Appendix A

SQUARE-WAVE PHASE GRATING

BIBLIOGRAPHY

- [1] L. A. Romero and F. M. Dickey. Mathematical aspects of laser beam shaping and splitting. page 765225.
- [2] Laser beam shaping: Theory and techniques.
- [3] Joseph W. Goodman. *Introduction to Fourier Optics*. Roberts & Co, 3rd ed edition. OCLC: ocm56632414.